JOURNAL OF GEOPHYSICAL RESEARCH, VOL. 106, NO. E10, PAGES 23,873–23,885, OCTOBER 25, 2001

Global mapping of Martian hematite mineral deposits: Remnants of water-driven processes on early Mars

P. R. Christensen,[1] R. V. Morris,[2] M. D. Lane,[2,3] J. L. Bandfield,[1,4] and M. C. Malin[5]

Abstract. Near-global (60°S to 60°N) thermal infrared mapping by the Thermal Emission Spectrometer (TES) on Mars Global Surveyor has revealed unique deposits of crystalline gray hematite (α-Fe_2O_3) exposed at the Martian surface in Sinus Meridiani, Aram Chaos, and in numerous scattered locations throughout Valles Marineris. The Sinus Meridiani material is an in-place, rock stratigraphic sedimentary unit characterized by smooth, friable layers composed primarily of basaltic sediments with ~10–15% crystalline gray hematite. This unit has outliers to the north that appear to have formed by stripping and removal. The hematite within Aram Chaos occurs in a sedimentary layer within a closed basin that was likely formed during the basin infilling and predates the formation of nearby chaos and outflow terrains. This unit appears to be exposed by erosion and may be more extensive beneath the surface. The Valles Marineris occurrences are closely associated with the interior layered deposits and may be in place within the layers or eroded sediments. Overall, crystalline gray hematite is extremely uncommon at the surface, yet in all observed locations it is closely associated with layered, sedimentary units. Here we argue that these hematite deposits have formed by a process involving chemical precipitation from aqueous fluids, under either ambient or hydrothermal conditions. Thus the TES mineralogic data provide evidence that liquid water has been stable at or near the surface, probably for millions of years by analogy with terrestrial iron formations, in specific locations on early Mars.

1. Introduction

Geomorphic evidence, accumulated from over 30 years of spacecraft observations, demonstrates that water erosion and transport occurred on the Martian surface (see reviews by *Sharp and Malin* [1975], *Baker* [1982], *Mars Channel Working Group* [1983], and *Baker et al.* [1992]). Viking Orbiter images [*Parker et al.*, 1989; *Parker et al.*, 1993; *Baker et al.*, 1991] and Mars Global Surveyor (MGS) topographic data [*Head et al.*, 1999] have been used to argue for the past existence of large bodies of standing water ("oceans") in the northern hemisphere, although the idea is controversial because shoreline features associated with these hypothesized oceans have not been observed in high-resolution MGS Mars Orbiter Camera (MOC) images [*Malin and Edgett*, 1999]. The geomorphic evidence alone, however, does not demonstrate the long-term stability of liquid water on the Martian surface. For example, many of the major channels likely formed in catastrophic events [*Sharp and Malin*, 1975; *Baker*, 1982; *Mars Channel Working Group*, 1983; *Baker et al.*, 1992], and basin infilling could have been followed by rapid freezing and/or sublimation.

Mineral deposits that are aqueous chemical precipitates or their evolved equivalents would provide direct evidence for the presence of liquid water in the Martian past. On the Earth, large-scale deposits of this type include carbonate and evaporite sequences and banded iron formations. A fundamental objective of the Thermal Emission Spectrometer (TES) instrument on the Mars Global Surveyor spacecraft [*Christensen et al.*, 1992] is to map the mineralogic composition of the Martian surface using infrared spectroscopy [*Farmer*, 1974; *Hunt et al.*, 1971; *Salisbury et al.*, 1987; *Blaney and McCord*, 1995; *Lane and Christensen*, 1997; *Bell*, 1996; *Christensen et al.*, 2000a]. We previously reported the initial detection of crystalline hematite in the equatorial region near Sinus Meridiani (centered near 2.5°S, 3°W) [*Christensen et al.*, 2000c]. Here we describe the global distribution, geologic context, and formation mechanisms of Martian hematite and the implications for near-surface water.

2. Identification and Mapping of TES Hematite

The TES instrument [*Christensen et al.*, 1992] is a Fourier transform Michelson interferometer operating with 10- or 5-cm^{-1} sampling in the thermal infrared spectral region from 1709 to 200 cm^{-1} (5.8 to 50 μm). Virtually all minerals have characteristic fundamental vibrational absorption bands is this spectral region [*Lyon*, 1962; *Lazarev*, 1972; *Farmer*, 1974; *Salisbury et al.*, 1987; *Salisbury*, 1993; *Lane and Christensen*, 1997; *Hamilton*, 2000; *Christensen et al.*, 2000a], making it well suited for mineralogic mapping. Spectral data are collected from six ~8.5 mrad instantaneous fields of view (IFOV) during a 2-s observation period. These IFOVs provide a contiguous strip three elements wide with a nominal spatial resolution of 3 km at an orbit altitude of 350 km.

TES spectra are calibrated to radiance using periodic views of space and an internal reference surface and converted to

[1]Department of Geological Sciences, Arizona State University, Tempe, Arizona.
[2]NASA Johnson Space Center, Houston, Texas.
[3]Now at Planetary Science Institute, Tucson, Arizona.
[4]Now at NASA GSFC, Greenbelt, Maryland.
[5]Malin Space Science Systems, San Diego, California.

Paper number 2000JE001415.
0148-0227/01/2000JE001415$09.00

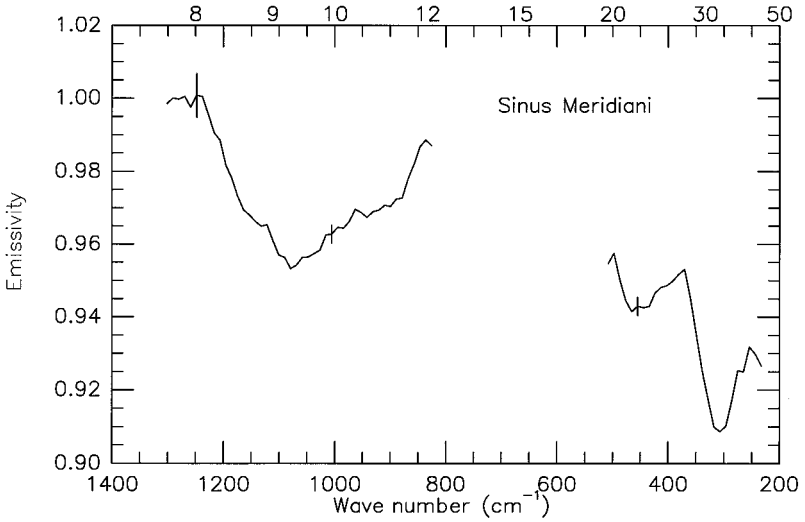

Figure 1. Thermal Emission Spectrometer (TES) atmosphere-corrected emissivity spectrum of the hematite-rich basaltic surface in Sinus Meridiani. Error bars of ±0.0025, ±0.0025, and ±0.006 correspond to the total estimated uncertainty, including instrument noise and uncertainties in the atmospheric correction, at 455, 1005, and 1248 cm^{-1}, respectively [*Christensen et al*., 2000b].

emissivity (ε). Ideally, emissivity is computed by dividing the calibrated radiance by the Planck function at the kinetic temperature of the surface. For TES analyses the surface kinetic temperature is approximated by deriving the brightness temperature from the TES calibrated radiance at each wave number and setting the kinetic temperature equal to the maximum brightness temperature within a wave number internal from 300 to 1350-cm^{-1}. This method assumes that the surface materials have unit emissivity at the point of maximum brightness temperature within the TES spectral range [*Christensen and Harrison*, 1993; *Ruff et al*., 1997]; this assumption has been demonstrated to be valid to within ~3% for a wide range of minerals, rocks, and soils [*Salisbury et al*., 1991; *Ruff et al*., 1997].

The TES instrument has a noise equivalent spectral radiance of $\sim 2.5 \times 10^{-8}$ W cm^{-2} sr^{-1}/cm^{-1} from ~300 to 1400 cm^{-1}, increasing to $\sim 6 \times 10^{-8}$ W cm^{-2} sr^{-1}/cm^{-1} at 250 cm^{-1} and to $\sim 4 \times 10^{-8}$ W cm^{-2} sr^{-1}/cm^{-1} at 1650 cm^{-1} [*Christensen*, 1999; *Christensen et al*., 2000b, 2001]. These random errors correspond to a noise equivalent delta emissivity (NE$\Delta\varepsilon$) of 0.004 at 1000 cm^{-1} and 0.002 at 400 cm^{-1} for a surface temperature of 275 K. Absolute radiometric accuracy was determined from prelaunch data to be better than 4×10^{-8} W cm^{-2} sr^{-1}/cm^{-1} [*Christensen et al*., 2001].

The TES data used in this paper are among the 55 million spectra collected during the MGS mapping phase over nearly 1 Mars year (aerocentric longitude, (L_s) 107° to 52°; orbits 1 through 8550; March 9, 1999, through September 19, 2000). Mapping phase data were collected at a local time at the equator of 13.90 hours (24 hours equal 1 Martian day). The methodology for separating the surface and atmospheric components of the radiance from Mars, which allows detailed analysis and interpretation of surface mineralogy [*Christensen et al*., 2000b; *Bandfield et al*., 2000a; *Christensen et al*., 2000c], is described previously by *Smith et al*. [2000] and *Bandfield et al*. [2000b]. The surface spectra closely match the spectral shape and contrast of laboratory spectra of both rock samples and linear mixtures of particulate (>~75 μm) minerals [*Christensen et al*., 2000b, 2000c; *Bandfield et al*., 2000a].

Atmosphere-removed TES spectra from the initial hematite discovery site in Sinus Meridiani [*Christensen et al*., 2000c] (Figure 1) show that the surface is composed primarily of basaltic material [*Christensen et al*., 2000b; *Bandfield et al*., 2000a] that has absorptions from 1250 to 680 cm^{-1} and 500 to 250 cm^{-1}. Mixed with this basaltic component is gray crystalline hematite that is uniquely identified by the presence of fundamental vibrational absorption features with emissivity minima centered near 300, 450, and >525 cm^{-1} and emissivity maxima centered near 370 and 500 cm^{-1} (Figure 2) [*Christensen et al*., 2000c]. Comparison of the Mars spectrum with a suite of oxide spectra shows that hematite provides an excellent match to both the position and shape of the two major absorption bands centered near 300 and 450 cm^{-1} (Figure 2). Hematite also provides a good match to the position and relative strength of the minor absorption bands at ~390 and 260 cm^{-1}.

The depth and shape of the hematite fundamental bands demonstrate that this hematite is crystalline and relatively coarse grained (>~10 μm), with diameters greater than hundreds of micrometers permitted within the measurement uncertainty and the natural spectral variability of hematite [*Christensen et al*., 2000c]. The areal abundance of hematite derived using the depth of the hematite absorption features corresponds to ~10–15% for coarse grains in the most concentrated occurrences in Sinus Meridiani. This derived abundance is consistent with the high abundance of basalt (>~80%) inferred from the deep 1250–850 cm^{-1} basalt absorption feature (Figure 1).

Crystalline and red hematite were previously reported as minor components (<5 wt% for ~100 nm diameter particles) in certain Martian bright regions using visible/near-IR spectral observations, and they, plus nanophase ferric oxide particles, are considered to give those regions their "red" color [*Morris et al*., 1997, 2000a; *Bell and Morris*, 1999; *Bell et al*., 1990]. Visible/near-IR spectral observations of the hematitic region of Sinus Meridiani are not characterized by the spectral signature of red hematite, implying that TES-detected hematite is gray (specular) hematite [*Bell and Morris*, 1999; *Christensen et al*., 2000c].

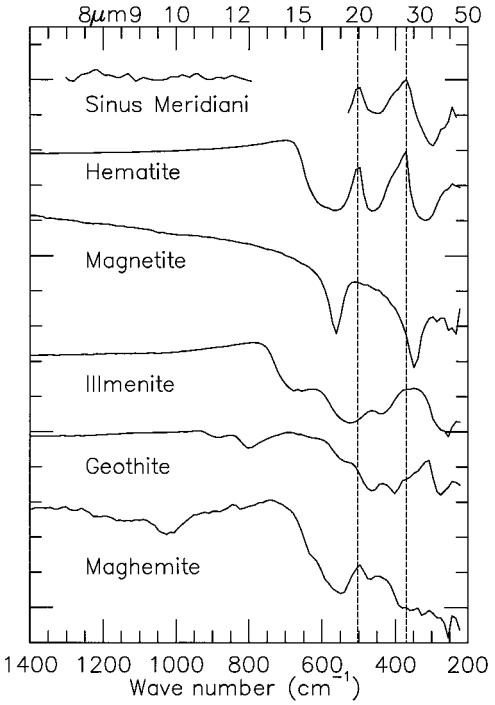

Figure 2. Comparison of a TES hematite spectrum (basalt component removed) with a suite of oxide spectra. The common oxides, including those shown here, can be readily identified by their IR spectra, and all but hematite can be eliminated as the dominant oxide in Sinus Meridiani.

In order to map the spatial distribution of gray, crystalline hematite a spectral index was defined using the major hematite absorption bands centered near 300 cm^{-1} and 450 cm^{-1} relative to the emissivity maximum near 375 cm^{-1} [*Christensen et al*., 2000c] (Figure 2). This parameter is given by $\varepsilon 2/(\varepsilon 1 + \varepsilon 3)$, where $\varepsilon 1$ is the average of TES bands 14–15 (band centers at 286–296 cm^{-1}); $\varepsilon 2$ is the average of bands 21–24 (360–391 cm^{-1}); and $\varepsilon 3$ is the average of bands 31–33 (466–476 cm^{-1}). The hematite index has been computed for all TES spectra with derived surface temperatures >230 K and emission angles <5°. These constraints were chosen to maximize the spectral quality and to reduce the spectral effects of atmospheric components. We estimate that the 1σ uncertainty in emissivity due to instrument noise, calibration errors, and atmospheric removal is approximately ±0.0025 in the 200 to 1000 cm^{-1} region [*Christensen et al*., 2001]. An average hematite index value of ~1.010 is typical for the vast majority of TES spectra, and variations in this index of ±0.002 are consistent with instrumental noise. The hematite-rich region in Sinus Meridiani has a peak index value that rises above the baseline value by a factor of >15 times the noise level. Inspection of individual spectra from different regions confirms that the spectral signature of hematite can be reliably detected under a wide range of observing conditions when the hematite index increases above a level of 1.018. Combining the measurement uncertainty with the variation in hematite spectral band depth with abundance indicates a detection limit of several percent corresponding to a hematite index of 1.018.

3. Global Hematite Mapping

Plate 1 shows the global distribution of gray hematite on Mars. This map provides the first near-global mineral map of Mars and shows that gray hematite is remarkably limited in occurrence at the surface. At a detection limit of several percent [*Christensen et al*., 2000c], gray hematite is only present in two large (>100 km diameter) areas, Sinus Meridiani (2°S, 4°W; Plate 2) and Aram Chaos (2°N, 21°W; Plate 3), along with numerous small (~10 km) occurrences scattered through the interior layered deposits in Valles Marineris (e.g., Plate 4). Estimated hematite areal abundances in these regions range from several percent to ~10–15%. The remainder of Mars from 60°S to 60°N, including red-hematite-bearing regions such as Olympus-Amazonis, is remarkably lacking in detectable crystalline gray hematite (Plate 1), although not all individual pixels with high index values have been manually inspected to see if they represent additional, small (<10 km) occurrences.

Gray hematite may be, or have been, more extensive than its present exposure, either as undetected subsurface units or through erosion of exposed units. However, given the extremely limited present exposures, it does not appear likely that hematite-rich rock units were commonly formed in Mars history. Instead, the limited occurrence of gray hematite suggests that its formation has required a unique combination of water abundance, temperature, pH, Eh, and rock composition that have only occurred rarely throughout Martian history.

4. Sinus Meridiani Region

The hematite-rich unit (Plate 2) correlates well with a distinct geomorphic unit that is smooth at the resolution limit of Viking Orbiter images (~30 m $pixel^{-1}$) and layered [*Edgett and Parker*, 1997]. This smooth surface expression is distinctly different from the surrounding heavily cratered terrain (Plate 2b), which contains features that are typical of the Martian southern highlands: ancient, eroded impact craters and a variety of branching, valley network troughs and valleys [*Edgett and Parker*, 1997; *Christensen et al*., 2000c]. *Edgett and Parker* [1997] argued that the smooth unit overlies, and is therefore younger than, the older heavily cratered material on the basis of embayment relationships apparent in Viking Orbiter images.

The boundary of the hematite-rich unit is abrupt, with the hematite index increasing from the background level to significant hematite absorption over a spatial distance of 1–2 TES pixels (5–10 km; Plate 2). The abrupt nature of this boundary, its excellent correlation with the smooth geomorphic unit, and the lack of wind tails or other evidence for aeolian transport all indicate that the hematite is not a mobile, surficial deposit but occurs within an in-place rock unit. These observations also suggest that hematite has not been significantly concentrated into a surface mantle and likely occurs at 5–15% abundance within the hematite-bearing layer.

A relatively fresh, unnamed 22 km crater located at 3°S, 6.6°W (Plate 2a, arrow) is superimposed on and postdates the formation of the hematite unit. The continuous ejecta blanket, which shows essentially no detectable evidence of hematite (Plate 2a), provides additional evidence that the hematite occurs as an in-place rock unit, as the hematite has not been redistributed across the crater ejecta despite the presence of dunes and wind streaks as evidence for aeolian transport within the region (Plate 2a).

MGS MOC images show that the hematite-bearing unit is remarkably smooth, with layers and mesas of stripped overlying layered units within the unit (Figure 3a) and internal lay-

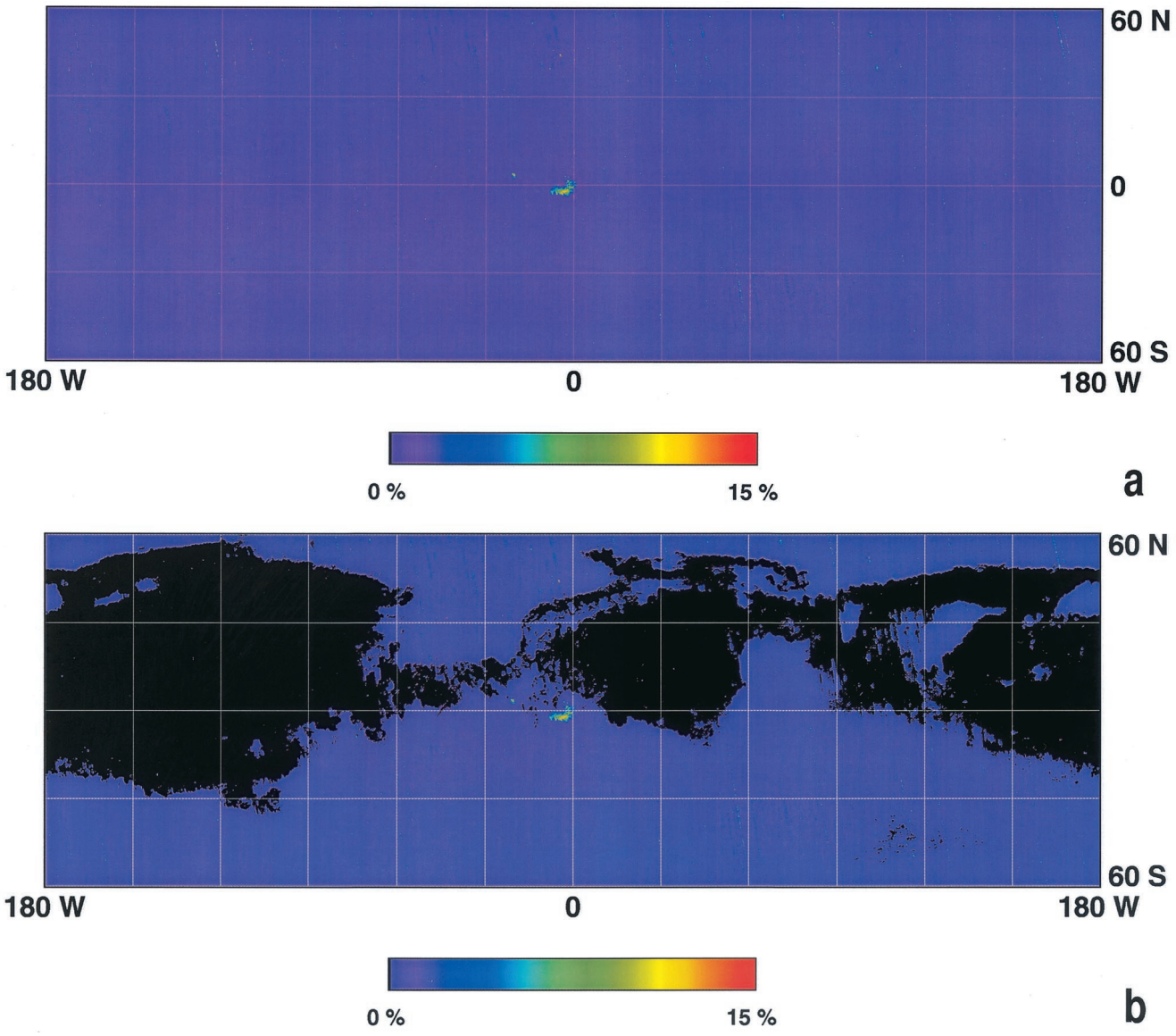

Plate 1. Global distribution of gray crystalline hematite on Mars. (a) Map from 60°S to 60°N produced by binning the hematite index in latitude and longitude at a scale (1/16° pixel^{-1}) that approximates the spatial resolution of individual TES pixels (3 × 6 km). The map has ~85% spatial coverage; unfilled bins were filled by linear interpolation between neighboring bins. (b) Image masked to exclude regions with an albedo >0.23 to eliminate bright, dust-covered surfaces where the surface composition is potentially dominated by aeolian dust.

ering visible along the eroded margin (Figure 3b). Individual layers vary in thickness, with indications of variations in strength based on the occurrence throughout the unit of both resistant, cliff-forming units and eroded, bench-forming units [*Christensen et al.*, 2000c]. The texture of erosion surfaces exposed in knobs, scarps, and ramps suggests that this unit is composed of materials that are easily eroded [*Edgett and Parker*, 1997; *Christensen et al.*, 2000c]. The most likely mechanism for the erosion of the layers is wind, suggesting that the material has little strength. There is no evidence for lava flow features, vents, or constructs on the hematite-bearing unit [*Edgett and Parker*, 1997]. From these characteristics we conclude that the hematite-bearing unit is sedimentary and not igneous in origin. TES spectra indicate that the sediments are basaltic in nature [*Christensen et al.*, 2000c, 2000b], implying that they are derived from older materials. The deep absorption features of this basalt [*Christensen et al.*, 2000b, Figure 1] indicates that the material currently at the surface is sand-sized or larger [e.g., *Salisbury and Wald*, 1992; *Ramsey and Christensen*, 1998]. Therefore, if these materials are sedimentary, then they are most likely coarse-grained, surface-transported sediments, rather than airfall.

Several isolated regions of high hematite abundance occur to the north of the main body (Plate 2). The distribution of these outliers and their morphology as observed in Viking images suggest that they are erosional remnants of a previously continuous layer that was greater in extent than its current distribution. Alternatively, these outliers may be erosional windows down to the hematite unit. In either case, it appears that the hematite unit was (or is) of greater extent than its current outcrop and that either the hematite unit, or material above it, is being stripped from this region. Once eroded, the hematite

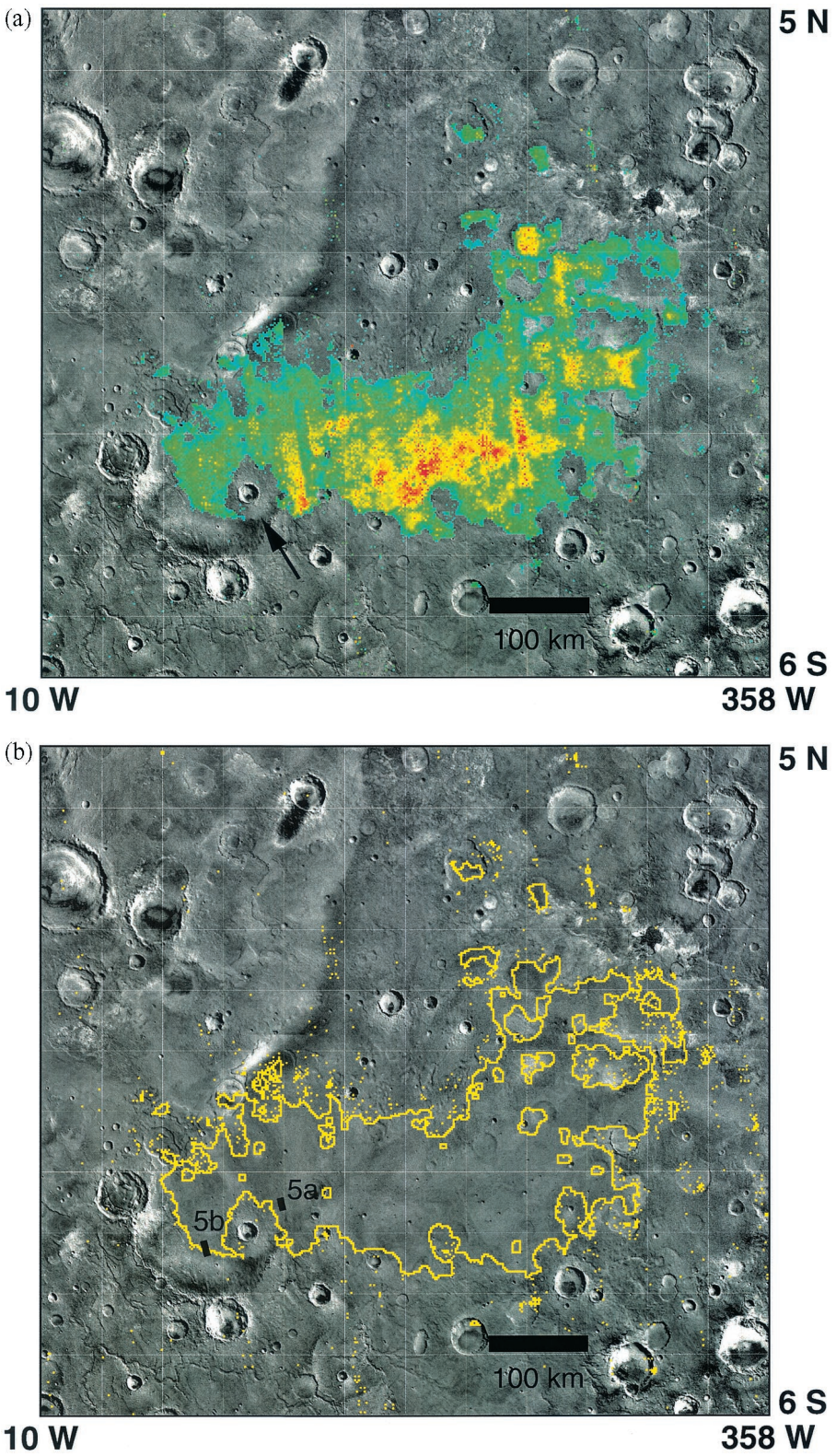

Plate 2. TES-derived hematite abundance in Sinus Meridiani. (a) TES-derived hematite abundance overlaid on a Viking base digital photomosaic image. Hematite index values of <1.018 have been made transparent to allow the underlying morphology to be visible. This value was chosen as a conservative upper limit of the TES detection limit (~2%) in the presence of instrument and atmospheric variability. Crater with ejecta blanket mantling the hematite unit is shown by arrow. (b) Outline of hematite-rich area showing geomorphology of underlying unit and excellent correlation with the smooth, layered unit that overlies the heavily cratered terrain. The locations of Figures 3a and 3b are indicated.

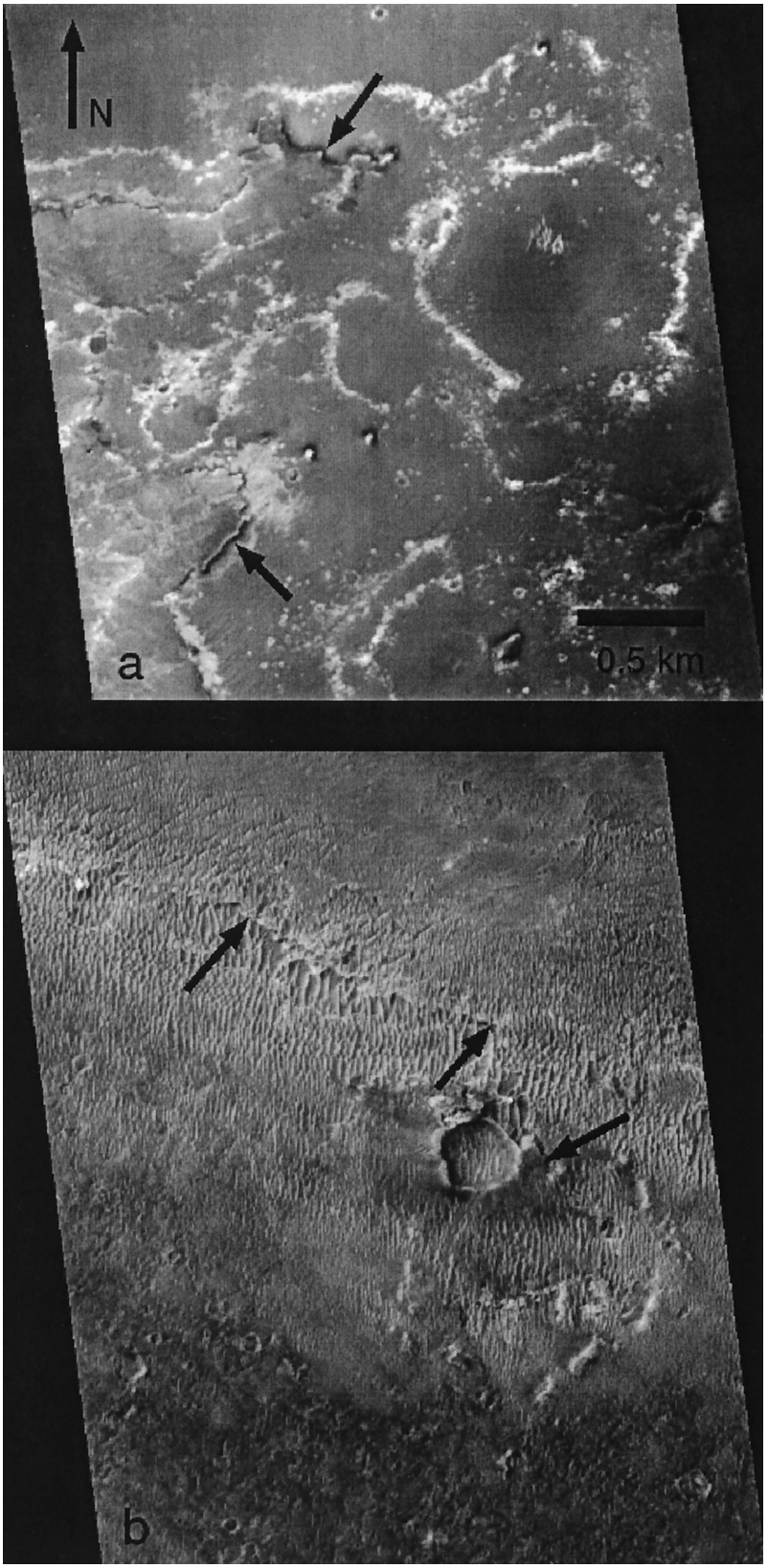

Figure 3. Mars Orbiter Camera (MOC) images of the Sinus Meridiani, hematite-rich surface. (a) Layering and mesas (arrows) within the TES Sinus Meridiani hematite unit. Subframe of MOC image M02-01539 is centered at 3.07°S, 6.03°W; subframe centered at ~2.7°S. Pixel width is 5.76 m, image width is 2.94 km. (b) Southwest margin of the Meridiani Formation. Note the scarps (arrows) that mark layering along the southern edge of the TES Sinus Meridiani hematite unit. Subframe of MOC image M03-00371 centered at 3.62°S, 7.23°W; subframe centered at ~3.25°S. Pixel width is 4.32 m, image width is 2.90 km.

must be mobile and readily dispersed by some mechanism as none is detected on the surrounding surfaces.

The stratigraphic distribution of crystalline gray hematite within the smooth unit can be inferred using the absence of detectable hematite within the continuous ejecta of the 22 km crater discussed above (Plate 2a, arrow). A general excavation-depth to transient-crater-diameter relationship suggests that a 20 km crater should excavate to approximately one tenth of the transient crater diameter [*Melosh*, 1989] and should produce concentric zones reflecting stratigraphic layers within the target material. It follows that the hematite-rich layer is considerably less than 1–2 km thick and is possibly confined to a thin surface layer.

On the basis of these observations we conclude that the hematite-rich material in Sinus Meridiani is a rock stratigraphic sedimentary formation, which we name the Meridiani Formation. It is the first rock formation identified by mineralogical composition on Mars, and its location differs, especially along the northern boundary, from the smooth unit ("sm") mapped by *Christensen et al*. [2000c] on the basis of morphology. The Meridiani Formation is interpreted to be sedimentary in origin and is characterized by friable layers composed primarily of basaltic sediments with ~10–15% crystalline hematite, has no large (>7 km), fresh craters, and is mappable over >175,000 km^2.

5. Aram Chaos

Crystalline gray hematite also occurs within a region ~60 km in diameter within the 280 km diameter crater Aram (Plate 3). This region has sharp boundaries, suggesting an in-place unit. Aram has been filled with substantial amounts of material following its formation, and nearby craters also show nearly complete infilling (Plate 3). The crater fill material is seen to be layered in both Viking and MOC images. We favor a sedimentary origin based upon the lack of lava flow features, vents, and constructs within the crater fill. We conclude that the hematite-rich materials in Aram Chaos are also associated with layered sedimentary deposits.

Outflow channels associated with chaos terrains are common in this area, indicating that there has been substantial surface and subsurface water in this region [*Sharp*, 1973; *Baker and Milton*, 1974; *Carr*, 1979]. There is evidence for incipient chaos formation and outflow associated with a relatively small (~15 km wide) channel that flows from Aram, but the size of this channel and the volume of material removed by outflow are modest in comparison to other nearby chaotic terrain (e.g., 0°N, 25°W; Plate 3, arrow). Nearby craters show only minor disruption and little or no removal of material by outflow channels. The hematite-rich region is not the topographically lowest area in the crater [*Smith et al*., 1999], so it appears unlikely that the hematite was formed or concentrated in a late-stage ponding event associated with the most recent channel formation.

Instead, we suggest that the hematite occurs within an in-place sedimentary layer composed primarily of basaltic sediments with 10–15% hematite within the Aram basin that was formed during the early infilling of this closed basin and predates the formation of the chaos and outflow terrains. Possibly the hematite-rich unit originally formed a continuous layer across Aram Chaos and may be present in nearby, filled craters.

6. Valles Marineris

Crystalline gray hematite has also been discovered in numerous small (5–20 km) areas in Valles Marineris (Plate 4a). The most extensive occurrences are within Ophir and Candor Chasma (Plate 4b), with numerous minor occurrences between 12°–13°S and 45°–50°W. The exact location of these materials relative to the surface morphology is difficult to determine owing to errors in existing maps. We have attempted to locate the TES spectra relative to the maps using the TES albedo channel as an independent means of matching surface features. Using this technique, it appears that the hematite-rich materials are associated with dark material located in topographic lows near the layered, friable deposits within Ophir and Candor [*McCauley*, 1978; *Lucchitta*, 1982; *Nedell et al*., 1987]. Red hematite has been reported previously in Candor [*Geissler et al*., 1993], but the locations do not agree with those observed by TES, and the visible/near-IR data for Candor may alternatively be due to poorly crystalline FeOOH polymorphs, including goethite, which has a band minimum near 900 nm and positive band depth near 520 nm [*Morris et al*., 2000a].

Hematite-rich materials are lacking in regions of the canyon system that do not have interior layered deposits, for example, in Ius and Coprates Chasma (Plate 4a). This relationship provides additional evidence that hematite formation is directly associated with the layered materials.

7. Spectral Properties

The spectral character of the hematite in Sinus Meridiani, Aram Chaos, and Candor Chasma is shown in Plate 5. The effects of atmospheric water ice and vapor, as well as the contribution from the other surface components, have been approximately removed by differencing the hematite-rich spectra from nearby (<100 km distant) spectra that do not show a hematite signature. Approximately 20 spectra were averaged for each orbit that covered each of the different regions; these orbit averages are shown in Plate 5. The minor variations in spectral properties within regions are consistent with the instrument noise ~0.0005 ε for averages of 20 spectra [*Christensen et al*., 2001] and variations in the atmospheric component. Incomplete removal of the atmospheric water vapor is particularly evident between 200 and 270 cm^{-1}.

Plate 6 shows a comparison of the average of all of the spectra for each of the regions shown in Plate 5. Comparison of these average spectra shows that there is little variation in spectral shape between these regions. We note the ~20-cm^{-1} shift in position of the 450 cm^{-1} band in the Aram Chaos materials relative to the other two regions. This shift is consistent with the measured variability in terrestrial hematite samples [*Morris et al*., 2000b]. The absolute depths of the hematite absorption bands, after correction for atmospheric and other surface components, are similar for these regions. Thus we conclude that the composition and maximum abundance of hematite in all three of these regions are similar.

Plate 7 shows a comparison of the average of the 27 5-cm^{-1} spectra collected to date for Sinus Meridiani with the 10-cm^{-1} data for the same area. No corrections for atmospheric or other surface components were applied to these data in order to allow a direct comparison of the effect of spectral resolution. We find that the primary differences are a better resolution of the water vapor bands in the 5-cm^{-1} data; no significant differences are seen in the spectral properties of the hematite surface component.

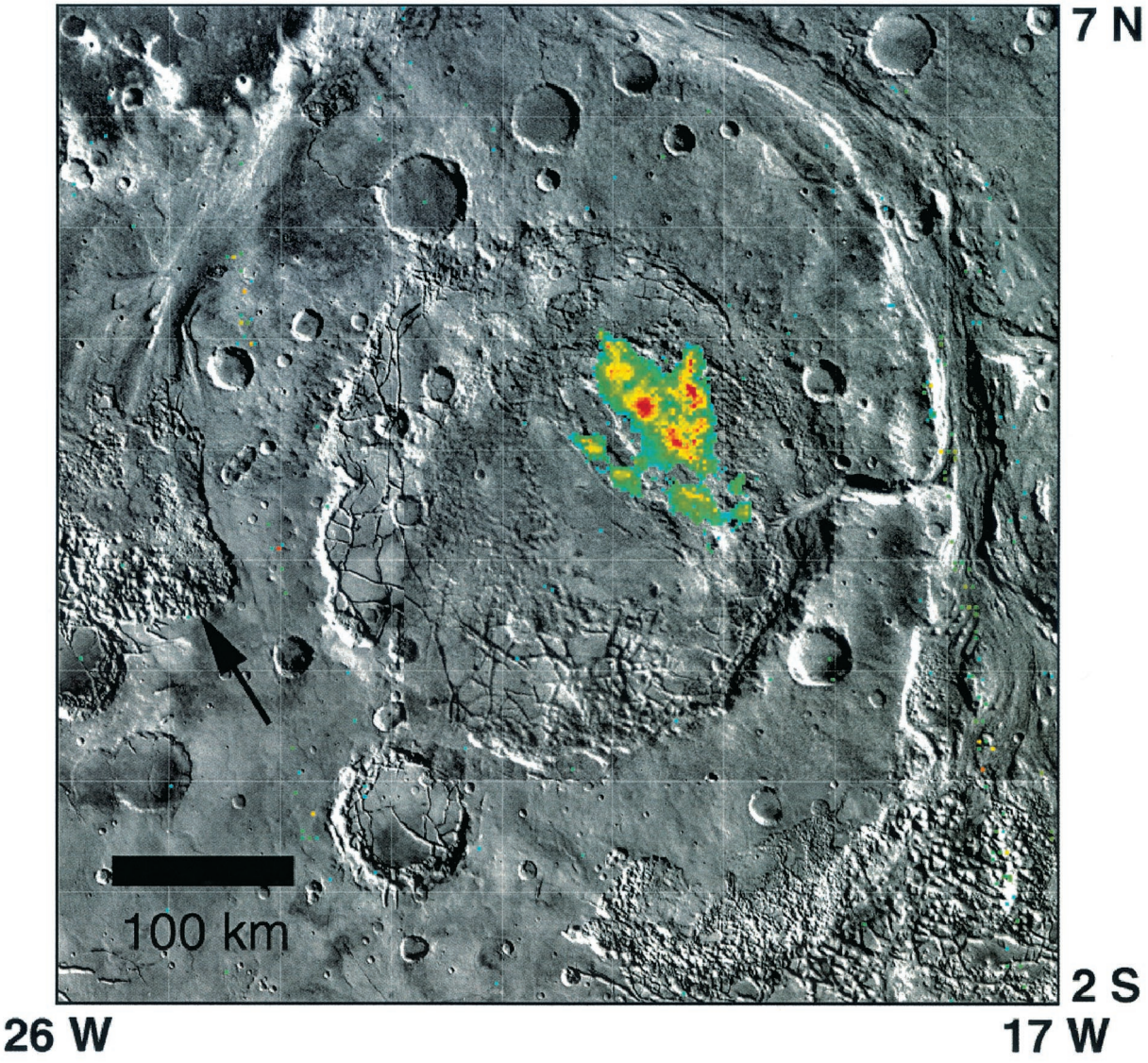

Plate 3. Distribution of gray crystalline hematite in Aram Chaos. Nearby chaotic terrain is shown by arrow. Hematite index values of <1.018 have been made transparent to allow the underlying morphology to be visible.

8. Hematite Formation Processes

Formation modes for gray hematite detected by TES can be grouped into two model classes: (1) chemical precipitation and (2) thermal oxidation of magnetite-rich lavas. Chemical precipitation models include model 1a, low-temperature precipitation of Fe oxides/oxyhydroxides from standing, oxygenated, Fe-rich water, followed by subsequent alteration to gray hematite; model 1b, low-temperature leaching of iron-bearing silicates and other materials to leave a Fe-rich residue (laterite style weathering), which is subsequently altered to gray hematite; model 1c, direct precipitation of gray hematite from Fe-rich circulating fluids of hydrothermal or other origin; and model 1d, formation of gray hematitic surface coatings during weathering. Note that models 1a and 1b require an oxidative alteration process (e.g., burial metamorphism) to convert Fe-oxide/oxide assemblages (e.g., red hematite, goethite, ferrihydrite, goethite, and siderite) to coarse-grained (>10 μm), gray hematite.

Although we exclude none of the above models, the geologic setting of the Martian hematite deposits, together with the terrestrial analogue samples, leads us to prefer certain models. The primary argument against thermal oxidation of magnetite-rich lavas (model 2) is the absence of distinct morphological evidence for lava flows or constructs and the presence of evidence for material more friable than primary lava in the Sinus Meridiani hematitic unit. Gray weathering rinds (model 1d) are not preferred on the basis of terrestrial experience in which red, and not gray, hematitic rinds are formed by weathering [e.g., *Cornell and Schwertmann*, 1996]. Finally, surface leaching and weathering, such as could occur in a moist oxidizing atmosphere or in regions of intense rainfall, are less consistent with the observed geomorphic associations and sharp boundaries. Typically, these processes produce diffuse units that crosscut geomorphic provinces.

Our preferred models are that the deposits of gray hematite formed by chemical precipitation from Fe-rich aqueous fluids,

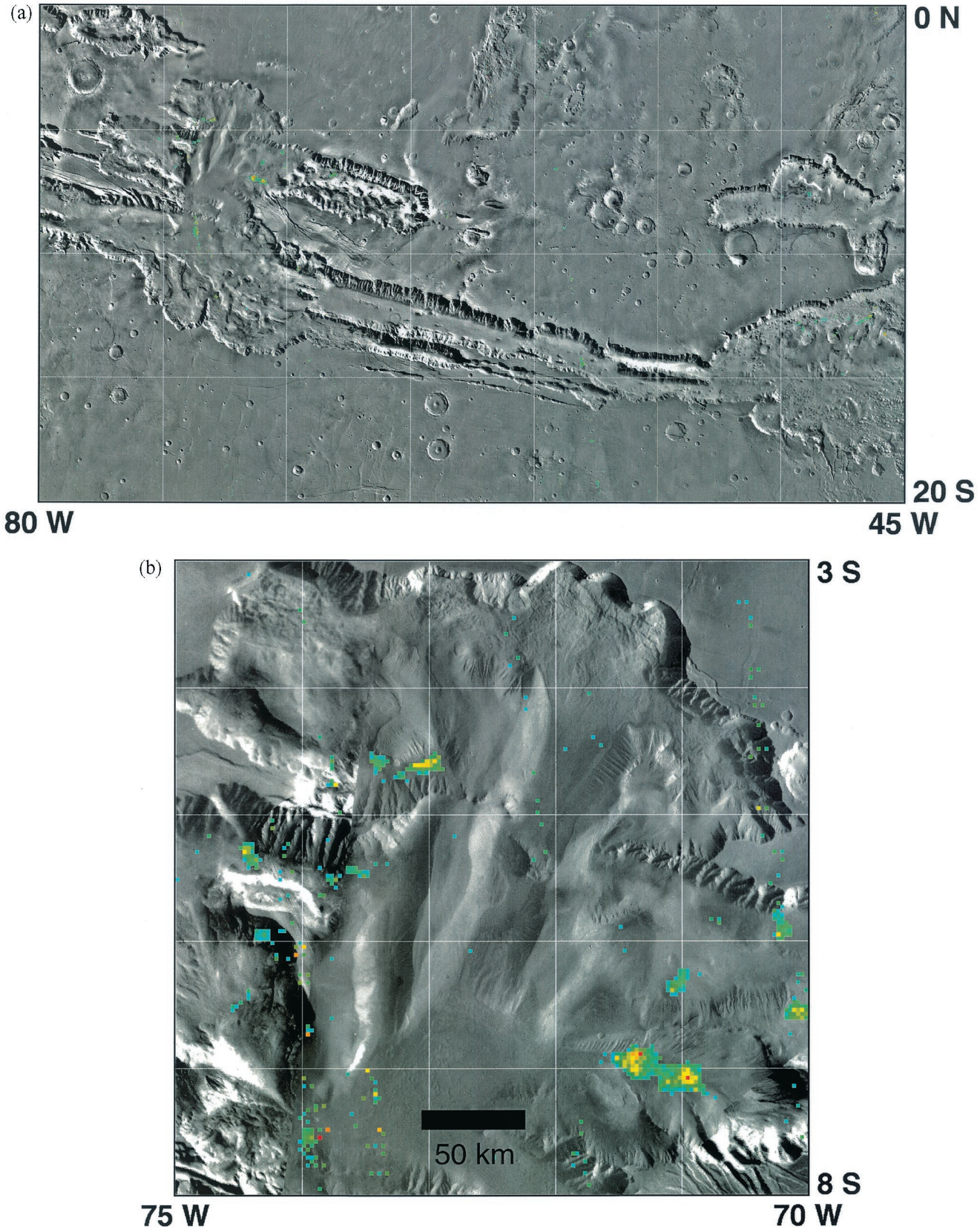

Plate 4. Distribution of gray crystalline hematite in the Valles Marineris region. Hematite index values of <1.018 have been made transparent to allow the underlying morphology to be visible. (a) A regional view of distribution of hematite in Valles Marineris. (b) A detailed view of hematite occurrence in Candor/Ophir Chasma.

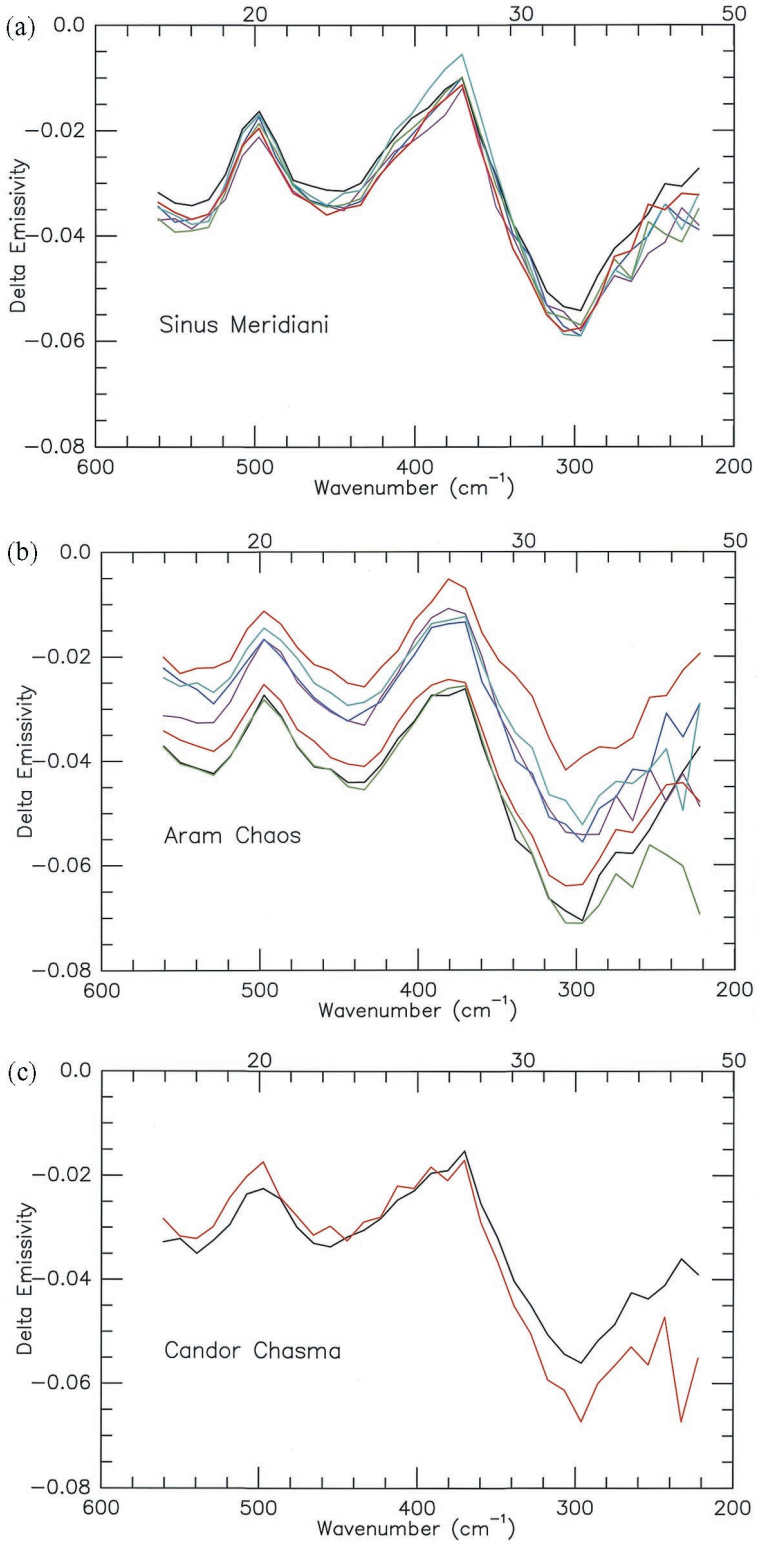

Plate 5. The spectral properties of gray crystalline hematite in (a) Sinus Meridiani, (b) Aram Chaos, and (c) Candor Chasma. Atmospheric and basaltic components have been removed by scaling to spectra acquired from regions ~100 km away outside the hematite-rich zones. (a) Data from orbits 2619, 4103, 4518, 5260, 5587, 5914, and 8555 selected from the region 2.6 to 2.2°S, 3.3 to 3.8°W. (b) Data from orbits 2016, 2695, 3110, 3764, 4506, 4921, 5248, and 8543 selected from the region 3.2 to 3.2°N, 20.2 to 20.8°W. (c) Data from orbits 6017 and 7325 selected from the region 7.2 to 6.7°S, 71.2 to 71.6°W.

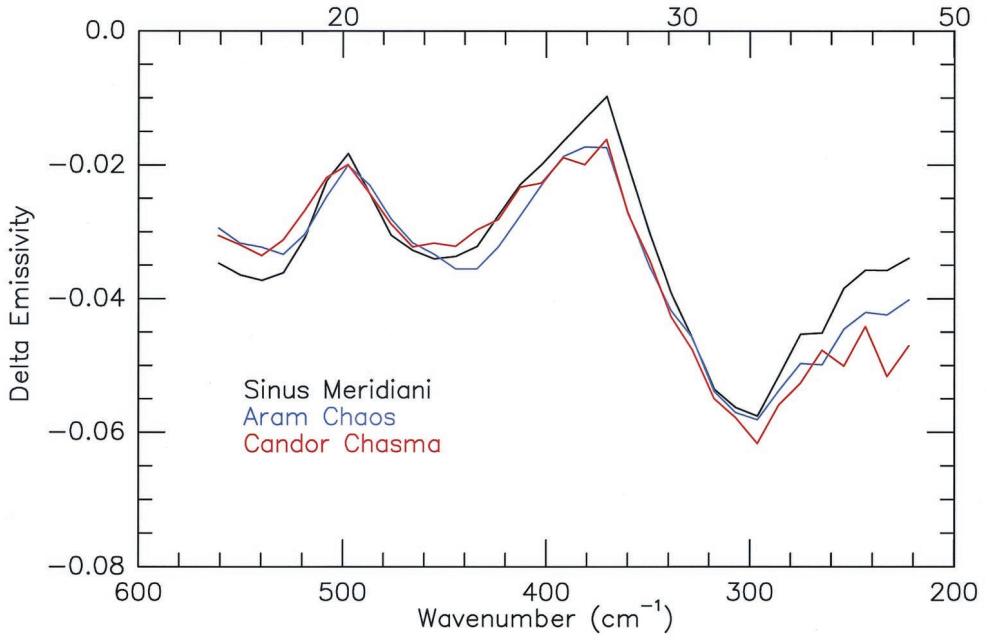

Plate 6. Comparison of the spectral properties of gray crystalline hematite in Sinus Meridiani, Aram Chaos, and Candor Chasma. The spectra shown are the averages of the spectra shown in Plate 5 for each of the regions. Note the similarity in the spectral character of hematite in these three regions.

under either ambient or hydrothermal conditions (models 1a and 1c). For model 1a a second step is required to coarsen the hematite [*Christensen et al*., 2000c]. Models involving aqueous processes are supported by the geologic context, which suggests that all three hematite sites are sedimentary environments. Hematite-bearing units in Aram and Valles Marineris occur in closed sedimentary basins consistent with deposition in water. Subsurface water has been present in Aram Chaos as evidenced by collapse and outflow features, and the hematite-bearing unit in Ophir/Candor is associated with layered, friable deposits that may be of aqueous origin [*McCauley*, 1978; *Lucchitta*, 1982; *Nedell et al*., 1987].

Precipitation under either ambient or hydrothermal conditions requires substantial amounts of liquid water and provides direct evidence for significant, long-term, water-driven processes. None of these sites show evidence for significant vertical uplift, implying that these aqueous processes occurred at or near the surface. Precipitation at ambient temperatures would suggest a large body of standing water to account for the areal extent of the deposits. Precipitation at hydrothermal temper-

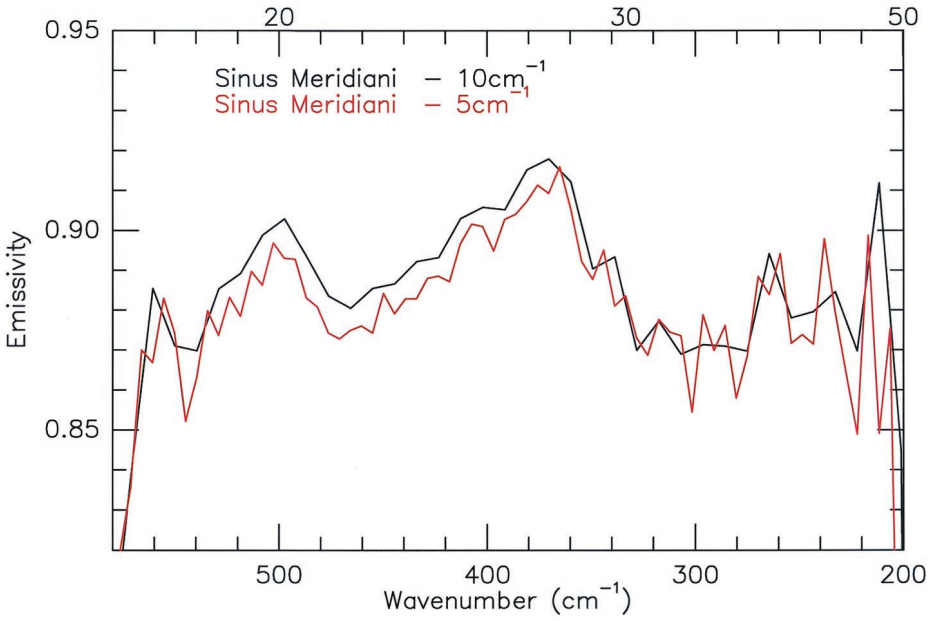

Plate 7. Comparison of spectra of the Sinus Meridiani region acquired at the nominal (10-cm^{-1}) TES spectral sampling and in high-resolution (5-cm^{-1}) mode. Atmospheric and basaltic components have been removed.

atures would require abundant hot water (but not necessarily standing water), perhaps in association with magmatic/tectonic activity, and access to a source rich in iron.

Possible terrestrial analogues for models 1a and 1c are iron formations which contain large deposits of massive or microplaty gray hematite [e.g., *Barley et al*., 1999; *James*, 1966]. The development of iron formations on Mars that are analogous to banded iron formations (BIFs) formed on the Earth during the Archean has been suggested by several authors [*Burns*, 1993; *Schaefer*, 1996; *Calvin*, 1998; *Christensen et al*., 2000c]. The origin of terrestrial BIFs remains a topic of debate (see review by *Guilbert and Frank* [1986]), but most proposed mechanisms (both inorganic and organically assisted) involve dissolution of large amounts of Fe^{2+} into anoxic water and subsequent deposition of iron-bearing phases when the level of dissolved oxygen increased, followed by alteration to convert the likely iron-bearing precipitates (e.g., goethite, ferrihydrite, and red hematite) to gray hematite. Terrestrial deposits are often associated with silica phases (e.g., quartz and chert) and/or carbonates which have not been detected anywhere on Mars, including the hematite regions [*Christensen et al*., 2001]. Perhaps the style of chemical precipitation on Mars, related to differences in chemical composition of circulating fluids and the chemical source regions for these fluids, is to precipitate predominantly Fe-bearing phases. Alternatively, by analogy with the giant BIF-hosted ore deposits at Hamersley, Australia, the silica-rich materials may have been removed by hydrothermal activity in association with magmatic/tectonic activity [*Barley et al*., 1999].

9. Implications for Stable, Liquid Water

The TES discovery of coarse, crystalline hematite in three, but only three, restricted locations that appear to be aqueous sedimentary environments has significant implications for the possibility of hydrothermal systems, ancient oceans, or lakes on Mars. At present there is no evidence from MGS TES for carbonates or phyllosilicates exposed at the surface of Mars at detection limits of ~10% [*Christensen et al*., 2001]. Thus there is no supportive TES evidence for the occurrence of regional oceans or seas [*Parker et al*., 1989; *Parker et al*., 1993; *Baker et al*., 1992; *Head et al*., 1999], although it remains possible that clay or carbonate minerals did not form in these seas or have since been buried or destroyed.

The results presented here do, however, provide evidence for aqueous mineralization, under either ambient or hydrothermal conditions, and indicate that liquid water was stable at or near the surface in specific locations on early Mars for substantial amounts of time. It is remarkable that the surface occurrence of detectable levels (>~2%) of crystalline gray hematite is limited to only two large and a small number of minor areas, although these units may have been more extensive within the equatorial region in the past or may still exist beneath the surface in extensive layered deposits. All of these areas are located within 15° of the equator. This distribution may be coincidental and related to erosional processes that have only exposed hematite deposits in these areas, or it may reflect an increased likelihood of liquid water occurring at warmer, equatorial latitudes. Overall, crystalline gray hematite is extremely uncommon at the surface, yet it is always closely associated with friable, layered, sedimentary units. This correlation provides evidence for a causal relationship; that is, crystalline gray hematite may only form on Mars in aqueous sedimentary environments.

Acknowledgments. The TES instrument was developed at the Santa Barbara Research Center, led by S. Silverman and M. Greenfield. G. Mehall, N. Gorelick, K. Bender, K. Homan, K. Feely, S. Anwar, and B. Steinberg supported the data acquisition and processing. V. Hamilton and S. Ruff provided assistance in the spectral and image analysis. P. Lucey provided helpful comments that improved the manuscript. We gratefully acknowledge the MGS spacecraft and mission operations teams at the Jet Propulsion Laboratory and Lockheed Martin Astronautics for their outstanding efforts in operating the spacecraft and acquiring science observations. The TES investigation is supported by the NASA Mars Exploration Program. R. V. M. was supported by the NASA Cosmochemistry Program. Contributed work was performed while M. D. L. held a National Research Council-JSC Research Associateship.

References

Baker, V. R., *The Channels of Mars*, Univ. of Texas Press, Austin, 1982.

Baker, V. R., and D. J. Milton, Erosion by catastrophic floods on Mars and Earth, *Icarus*, *23*, 27–41, 1974.

Baker, V. R., R. G. Strom, V. C. Gulick, J. S. Kargel, G. Komatsu, and V. S. Kale, Ancient oceans, ice sheets, and the hydrological cycle on Mars, *Nature*, *352*, 589–862, 1991.

Baker, V. R., M. H. Carr, V. C. Gulick, C. R. Williams, and M. S. Marley, Channels and valley networks, in *Mars*, edited by H. H. Kieffer et al., pp. 493–522, Univ. of Ariz. Press, Tucson, 1992.

Bandfield, J. L., V. E. Hamilton, and P. R. Christensen, A global view of Martian volcanic compositions, *Science*, *287*, 1626–1630, 2000a.

Bandfield, J. L., M. D. Smith, and P. R. Christensen, Spectral dataset factor analysis and end-member recovery: Application to analysis of Martian atmospheric particulates, *J. Geophys. Res*., *105*, 9573–9587, 2000b.

Barley, M. E., A. L. Pickard, S. G. Hagemann, and S. L. Folkert, *Nature*, *34*, 784–789, 1999.

Bell, J. F., III, Iron, sulfate, carbonate, and hydrated minerals on Mars, in *Mineral Spectroscopy: A Tribute to Roger G. Burns*, edited by M. D. Dyar, C. McCammon, and M. W. Schaefer, *Spec. Publ. Geochem. Soc*., *5*, 359–380, 1996.

Bell, J. F., III, and R. V. Morris, Identification of hematite on Mars from HST, *Lunar Planet. Sci*., *XXX*, abstract 1751, 1999.

Bell, J. F., III, T. B. McCord, and P. D. Owensby, Observational evidence of crystalline iron oxides on Mars, *J. Geophys. Res*., *95*, 14,447–14,461, 1990.

Blaney, D. L., and T. B. McCord, Indications of sulfate minerals in the martian soil from Earth-based spectroscopy, *J. Geophys. Res*., *100*, 14,433–14,441, 1995.

Burns, R. G., Rates and mechanisms of chemical weathering of ferromagnesian silicate minerals on Mars, *Geochim. Cosmochim. Acta*, *57*, 4555–4574, 1993.

Calvin, W. M., Could Mars be dark and altered?, *Geophys. Res. Lett*., *25*, 1597–1600, 1998.

Carr, M. H., Formation of martian flood features by release of water from confined aquifers, *J. Geophys. Res*., *84*, 2995–3007, 1979.

Christensen, P. R., Calibration report for the Thermal Emission Spectrometer (TES) for the Mars Global Surveyor Mission, Mars Global Surveyor Project, Jet Propul. Lab., Pasadena, Calif., 1999.

Christensen, P. R., and S. T. Harrison, Thermal infrared emission spectroscopy of natural surfaces: Application to desert varnish coatings on rocks, *J. Geophys. Res*., *98*, 19,819–19,834, 1993.

Christensen, P. R., et al., Thermal Emission Spectrometer experiment: Mars Observer mission, *J. Geophys. Res*., *97*, 7719–7734, 1992.

Christensen, P. R., J. L. Bandfield, V. E. Hamilton, D. A. Howard, M. D. Lane, J. L. Piatek, S. W. Ruff, and W. L. Stefanov, A thermal emission spectral library of rock forming minerals, *J. Geophys. Res*., *105*, 9735–9738, 2000a.

Christensen, P. R., J. L. Bandfield, M. D. Smith, V. E. Hamilton, and R. N. Clark, Identification of a basaltic component on the Martian surface from Thermal Emission Spectrometer data, *J. Geophys. Res*., *105*, 9609–9621, 2000b.

Christensen, P. R., et al., Detection of crystalline hematite mineralization on Mars by the Thermal Emission Spectrometer: Evidence for near-surface water, *J. Geophys. Res*., *105*, 9623–9642, 2000c.

Christensen, P. R., et al., The Mars Global Surveyor Thermal Emission Spectrometer experiment: Investigation description and surface science results, *J. Geophys. Res*., this issue.

Cornell, R., and U. Schwertmann, *The Iron Oxides: Structure, Properties, Reactions, Occurrence, and Uses*, 573 pp., John Wiley, New York, 1996.

Edgett, K. S., and T. J. Parker, Water on early Mars: Possible subaqueous sedimentary deposits covering ancient cratered terrain in western Arabia and Sinus Meridiani, *Geophys. Res. Lett*., *24*, 2897–2900, 1997.

Farmer, V. C., *The Infrared Spectra of Minerals*, 539 pp., Mineral. Soc., London, 1974.

Geissler, P. E., R. B. Singer, G. Komatsu, S. Murchie, and J. Mustard, An unusual spectral unit in West Candor Chasma: Evidence for aqueous or hydrothermal alteration in the Martian canyons, *Icarus*, *106*, 380–391, 1993.

Guilbert, J. M., and C. F. Frank Jr., *The Geology of Ore Deposits*, W. H. Freeman, New York, 1986.

Hamilton, V. E., Thermal infrared emission spectroscopy of the pyroxene mineral series, *J. Geophys. Res*., *105*, 9701–9716, 2000.

Head, J. W., III, H. Hiesinger, M. A. Ivanov, and M. A. Kreslavsky, Possible ancient oceans on Mars: Evidence from Mars Orbiter Laser altimeter data, *Science*, *286*, 2134–2137, 1999.

Hunt, G. R., J. W. Salisbury, and C. J. Lenhoff, Visible and near-infrared spectra of minerals and rocks, III, Oxides and hydroxides, *Mod. Geol*., *2*, 195–205, 1971.

James, H. L., *Data of Geochemistry*, *U.S. Geol. Surv. Prof. Pap*., *440-W*, 1966.

Lane, M. D., and P. R. Christensen, Thermal infrared emission spectroscopy of anhydrous carbonates, *J. Geophys. Res*., *102*, 25,581–25,592, 1997.

Lazarev, A. N., *Vibrational Spectra and Structure of Silicates*, translated from Russian by G. D. Archard, 302 pp., Consult. Bur., New York, 1972.

Lucchitta, B. K., Lakes or playas in Valles Marineris, in *Reports of Planetary Geology Program*, *NASA Tech. Memo*., *TM-85127*, 233–234, 1982.

Lyon, R. J. P., Evaluation of infrared spectroscopy for compositional analysis of lunar and planetary soils, Final Report Under Contract NASr-49, 139 pp., Stanford Res. Inst., Menlo Park, Calif., 1962.

Malin, M. C., and K. S. Edgett, Oceans or seas in the Martian northern lowlands: High-resolution imaging tests of proposed coastlines, *Geophys. Res. Lett*., *26*, 3049–3052, 1999.

Mars Channel Working Group, Channels and valleys on Mars, *Geol. Soc. Am. Bull*., *94*, 1035–1054, 1983.

McCauley, J. F., Geologic map of the Coprates Quadrangle of Mars, scale 1:5,000,000, *U.S. Geol. Surv. Misc. Invest. Map*, *I-897*, 1978.

Melosh, H. J., *Impact Cratering, A Geologic Process*, 78 pp., Oxford Univ. Press, New York, 1989.

Morris, R. V., D. C. Golden, and J. F. Bell III, Low-temperature reflectivity spectra of red hematite and the color of Mars, *J. Geophys. Res*., *102*, 9125–9133, 1997.

Morris, R. V., et al., Mineralogy, composition, and alteration of Mars Pathfinder rocks and soils: Evidence from multispectral elemental, and magnetic data on terrestrial analogue, SNC meteorite, and Pathfinder samples, *J. Geophys. Res*., *105*, 1757–1817, 2000a.

Morris, R. V., M. D. Lane, S. Mertzman, T. D. Shelfer, and P. R. Christensen, Chemical and mineralogical purity of Sinus Meridiani hematite, *Lunar Planet. Sci*. [CD-ROM], *XXXI*, abstract 1618, 2000b.

Nedell, S. S., S. W. Squyres, and D. W. Anderson, Origin and evolution of the layered deposits in the Valles Marineris, Mars, *Icarus*, *70*, 409–441, 1987.

Parker, T. J., D. S. Gorsline, R. S. Saunders, D. C. Pieri, and D. M. Schneeberger, Coastal geomorphology of the Martian northern plains, *J. Geophys. Res*., *98*, 11,061–11,078, 1993.

Parker, T. S., R. S. Saunders, and D. M. Schneeberger, Transitional morphology in the west dueteronilus Mensae region of Mars: Implications for modification of the lowland/upland boundary, *Icarus*, *82*, 111–145, 1989.

Ramsey, M. S., and P. R. Christensen, Mineral abundance determination: Quantitative deconvolution of thermal emission spectra, *J. Geophys. Res*., *103*, 577–596, 1998.

Ruff, S. W., P. R. Christensen, P. W. Barbera, and D. L. Anderson, Quantitative thermal emission spectroscopy of minerals: A technique for measurement and calibration, *J. Geophys. Res*., *102*, 14,899–14,913, 1997.

Salisbury, J. W., Mid-infrared spectroscopy: Laboratory data, in *Remote Geochemical Analysis: Elemental and Mineralogical Composition*, edited by C. Pieters and P. Englert, pp. 79–98, Cambridge Univ. Press, New York, 1993.

Salisbury, J. W., and A. Wald, The role of volume scattering in reducing spectral contrast of reststrahlen bands in spectra of powdered minerals, *Icarus*, *96*, 121–128, 1992.

Salisbury, J. W., L. S. Walter, and N. Vergo, Mid-infrared (2.1–25 μm) spectra of minerals, First Edition, *U.S. Geol. Surv. Open File Rep*., *87-263*, 1987.

Salisbury, J. W., L. S. Walter, N. Vergo, and D. M. D'Aria, *Infrared (2.1–25 μm) Spectra of Minerals*, 267 pp., Johns Hopkins Univ. Press, Baltimore, Md., 1991.

Schaefer, M. W., Are there abiotically-precipitated iron-formations on Mars?, in *Mineral Spectroscopy: A Tribute to Roger G. Burns*, edited by M. D. Dyar, C. McCammon, and M. W. Schaefer, *Spec. Publ. Geochem. Soc*., *5*, 381–393, 1996.

Sharp, R. P., Mars: Fretted and chaotic terrains, *J. Geophys. Res*., *78*, 4073–4083, 1973.

Sharp, R. P., and M. C. Malin, Channels on Mars, *Geol. Soc. Am. Bull*., *86*, 593–609, 1975.

Smith, D. E., et al., The global topography of Mars and implications for surface evolution, *Science*, *284*, 1495–1503, 1999.

Smith, M. D., J. L. Bandfield, and P. R. Christensen, Separation of atmospheric and surface spectral features in Mars Global Surveyor Thermal Emission Spectrometer (TES) spectra: Models and atmospheric properties, *J. Geophys. Res*., *105*, 9589–9608, 2000.

J. L. Bandfield, NASA GSFC, Code 693.0, Building 2, Room 130D, Greenbelt, MD 20771. (jbandfield@lepvax.gsfc.nasa.gov)

P. R. Christensen, Department of Geological Sciences, Arizona State University, Box 871404, Tempe, AZ 85287-1404. (phil.christensen@asu.edu)

M. D. Lane, The Planetary Science Institute, Tucson Division, 620 North Sixth Avenue, Tucson, AZ 85705-8331. (melissalanebergh@yahoo.com)

M. C. Malin, Malin Space Science Systems, P.O. Box 91048, San Diego, CA 92191-0148. (malin@msss.com)

R. V. Morris, NASA Johnson Space Center, MC SN3, Houston, TX 77058. (richard.v.morris1@jsc.nasa.gov)

(Received October 25, 2000; revised February 6, 2001;
accepted February 8, 2001.)